Identification of a Primary Target of Thalidomide Teratogenicity

Takumi Ito *et al.*

Science **327**, 1345 (2010);
DOI: 10.1126/science.1177319

Science (print ISSN 0036-8075; online ISSN 1095-9203) is published weekly, except the last week in December, by the American Association for the Advancement of Science, 1200 New York Avenue NW, Washington, DC 20005.

Identification of a Primary Target of Thalidomide Teratogenicity

Takumi Ito,[1]* Hideki Ando,[2]* Takayuki Suzuki,[3,4] Toshihiko Ogura,[3] Kentaro Hotta,[2] Yoshimasa Imamura,[5] Yuki Yamaguchi,[2] Hiroshi Handa[1,2]†

Half a century ago, thalidomide was widely prescribed to pregnant women as a sedative but was found to be teratogenic, causing multiple birth defects. Today, thalidomide is still used in the treatment of leprosy and multiple myeloma, although how it causes limb malformation and other developmental defects is unknown. Here, we identified cereblon (CRBN) as a thalidomide-binding protein. CRBN forms an E3 ubiquitin ligase complex with damaged DNA binding protein 1 (DDB1) and Cul4A that is important for limb outgrowth and expression of the fibroblast growth factor Fgf8 in zebrafish and chicks. Thalidomide initiates its teratogenic effects by binding to CRBN and inhibiting the associated ubiquitin ligase activity. This study reveals a basis for thalidomide teratogenicity and may contribute to the development of new thalidomide derivatives without teratogenic activity.

During the late 1950s and early 1960s, thalidomide was sold as a sedative in over 40 countries and was often prescribed to pregnant women as a treatment for morning sickness. Before its teratogenic activity came to light and its use was discontinued, ~10,000 affected children were born from women taking thalidomide during pregnancy (*1*–*3*). Use of thalidomide during weeks 3 to 8 of gestation causes multiple birth defects such as limb, ear, cardiac, and gastrointestinal malformations (*1*–*3*). The limb malformations, known as phocomelia and amelia, are characterized, respectively, by severe shortening or complete absence of legs and/or arms, whereas the ear malformations lead to anotia, microtia, and hearing loss. Despite considerable effort, little is known about how these developmental defects are caused. Previous studies have suggested thalidomide-induced oxidative stress and its antiangiogenic action as a possible cause of teratogenicity (*4*, *5*). However, several important questions remain unanswered, such as what are direct targets of thalidomide and how the target molecules mediate its teratogenic effects.

Recently, thalidomide use has increased for the treatment of multiple myeloma and erythema nodosum leprosum, a painful complication of leprosy (*2*, *3*, *6*, *7*). Owing to its teratogenicity, however, thalidomide is used under strict control (*8*), and removal of its side effects is desirable for wider applications of this potentially useful drug. It is important to elucidate the molecular mechanism of thalidomide teratogenicity, especially to identify its molecular target(s), because such knowledge might allow rapid screening for potentially useful related compounds devoid of teratogenic activity. In this regard, we have been developing high-performance affinity beads that allow single-step affinity purification of drug target proteins from crude cell extracts (*9*). Here we show that cereblon (CRBN), a protein encoded by a candidate gene for mild mental retardation, is a primary target of thalidomide teratogenicity.

Binding of thalidomide to CRBN and DDB1. To purify thalidomide-binding proteins, we performed affinity purification using ferrite-glycidyl methacrylate (FG) beads (*9*). The carboxylic thalidomide derivative FR259625 was covalently conjugated to the beads (fig. S1) and incubated with human HeLa cell extracts (*10*). After extensive washing, bound proteins were eluted with free thalidomide, and the eluate fractions were subjected to SDS gel electrophoresis and silver staining. Two polypeptides were specifically eluted (Fig. 1A, lane 3). When free thalidomide was added to extracts before incubation with the beads, the yields of these proteins were reduced (Fig. 1A, lane 4), which suggested that these proteins specifically interact with thalidomide. The 127- and 55-kD proteins were therefore subjected to proteolytic digestion and tandem mass spectrometry and were identified as CRBN and damaged DNA binding protein 1 (DDB1), respectively (table S1). Identities of these proteins were confirmed by immunoblotting (Fig. 1A). CRBN and DDB1 were isolated similarly as thalidomide-binding proteins from various cell types (fig. S2). To determine whether this interaction is direct, we used purified recombinant proteins. FLAG-tagged CRBN, but not V5 (GKPIPNPLLGLDST) (*11*) epitope- and histidine (His)–tagged DDB1, bound to thalidomide beads (Fig. 1B). We therefore asked whether DDB1 binds to thalidomide beads through its interaction with CRBN. As expected, DDB1 was coprecipitated with FLAG- and hemagglutinin (HA) epitope–tagged (FH-) CRBN (Fig. 1C) and was not affinity-purified from CRBN-depleted 293T cells (fig.

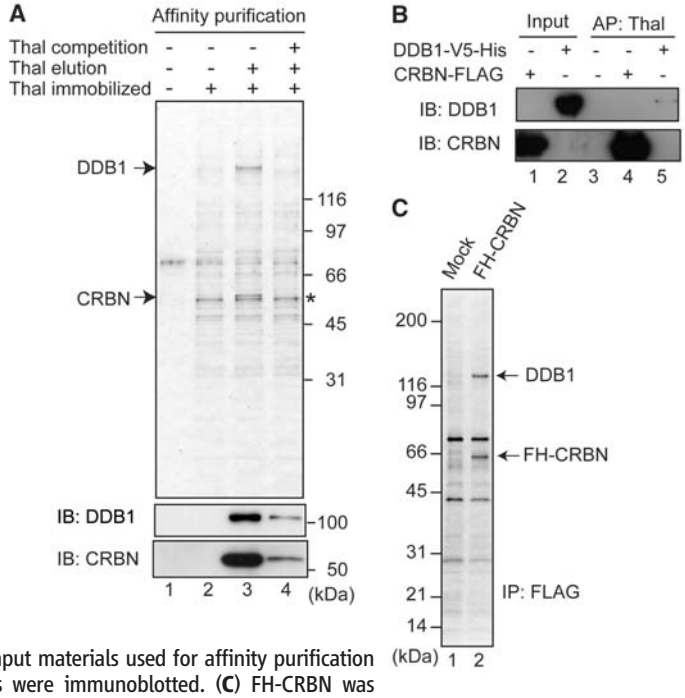

Fig. 1. Thalidomide binds to CRBN and DDB1. (**A**) Thalidomide (Thal)-binding proteins were purified from HeLa cell extracts by using thalidomide-immobilized (+) or control (–) beads. Where indicated, bound proteins were eluted with free thalidomide. As indicated, 0.3 mM thalidomide was added to extracts before incubation with the beads. Eluted proteins were analyzed by silver staining (top) or immunoblotting (IB) (bottom). Asterisk indicates nonspecific signal. (**B**) Purified recombinant CRBN-FLAG and DDB1-V5-His were, respectively, incubated with thalidomide beads. Input materials used for affinity purification (AP) and bound materials were immunoblotted. (**C**) FH-CRBN was immunoprecipitated (IP) from 293T cells stably expressing FH-CRBN or from control cells, followed by SDS gel electrophoresis and silver staining.

[1]Integrated Research Institute, Tokyo Institute of Technology, Yokohama 226-8503, Japan. [2]Graduate School of Bioscience and Biotechnology, Tokyo Institute of Technology, Yokohama 226-8501, Japan. [3]Institute of Development, Aging and Cancer, Tohoku University, Sendai 980-8575, Japan. [4]Precursory Research for Embryonic Science and Technology, Japan Science and Technology Agency (JST), Saitama 332-0012, Japan. [5]Drug Discovery Research, Astellas Pharma Inc., Ibaraki 305-8585, Japan.

*These authors contributed equally to this work.
†To whom correspondence should be addressed. E-mail: handa.h.aa@m.titech.ac.jp

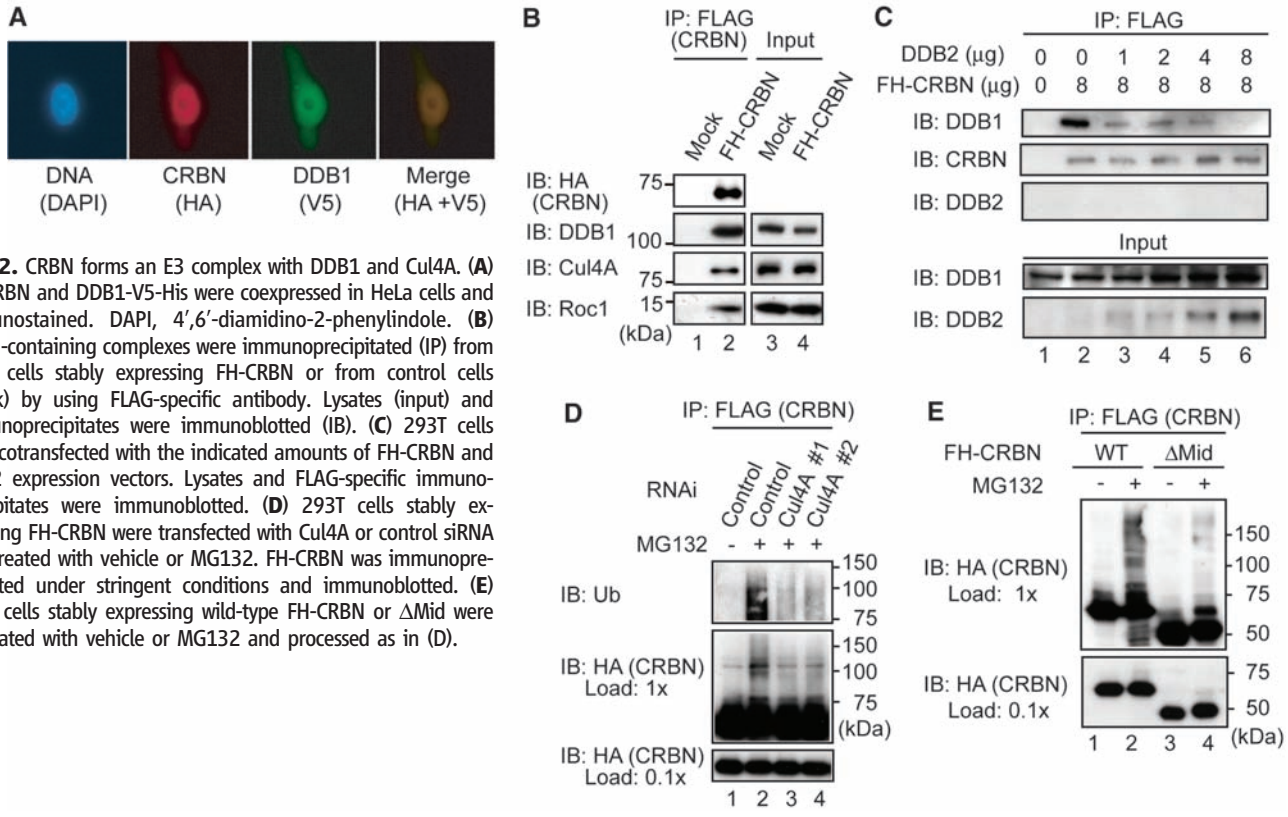

Fig. 2. CRBN forms an E3 complex with DDB1 and Cul4A. (**A**) FH-CRBN and DDB1-V5-His were coexpressed in HeLa cells and immunostained. DAPI, 4′,6′-diamidino-2-phenylindole. (**B**) CRBN-containing complexes were immunoprecipitated (IP) from 293T cells stably expressing FH-CRBN or from control cells (mock) by using FLAG-specific antibody. Lysates (input) and immunoprecipitates were immunoblotted (IB). (**C**) 293T cells were cotransfected with the indicated amounts of FH-CRBN and DDB2 expression vectors. Lysates and FLAG-specific immunoprecipitates were immunoblotted. (**D**) 293T cells stably expressing FH-CRBN were transfected with Cul4A or control siRNA and treated with vehicle or MG132. FH-CRBN was immunoprecipitated under stringent conditions and immunoblotted. (**E**) 293T cells stably expressing wild-type FH-CRBN or ΔMid were incubated with vehicle or MG132 and processed as in (D).

S3A), which led us to conclude that thalidomide interacts directly with CRBN and indirectly with DDB1 through its interaction with CRBN. The equilibrium dissociation constant of the CRBN-thalidomide interaction was calculated to be 8.5 nM (*10*). Moreover, CRBN did not bind to phthalimide, a nonteratogenic analog of thalidomide (*12*), which substantiated the high affinity and specificity of the CRBN-thalidomide interaction (fig. S3B).

Formation of an E3 complex by CRBN, DDB1, and Cul4A. Human *CRBN* was originally identified as a candidate gene for autosomal recessive mild mental retardation and encodes a 442–amino acid protein that is highly conserved from plants to humans (*13*). Although CRBN was reported to interact with DDB1 in a recent proteomic analysis (*14*), the functional relevance of this interaction remains unclear. Consistent with the apparently stoichiometric interaction of CRBN and DDB1 (Fig. 1C), these proteins are colocalized mainly in the nucleus, but also in the cytoplasm (Fig. 2A). DDB1 is a component of E3 ubiquitin ligase complexes containing Cullin 4 (Cul4A or Cul4B), regulator of cullins 1 (Roc1), and a substrate receptor (*15*, *16*). In principle, the function of E3 ubiquitin ligases is to direct the polyubiquitination of substrate proteins by a specifically interacting ubiquitin-conjugating enzyme (E2) (*17*, *18*). Cul4 is thought to play a scaffold function, whereas Roc1 has a RING finger domain that associates with the E2 ubiquitin-conjugating enzyme. Substrate receptors, such as DDB2, CSA, and CDT2, directly bind to specific substrates and mediate their ubiquitination (*15*, *19*, *20*). We examined whether CRBN interacts with other components of the E3 complex and found that Cul4A and Roc1 were indeed coprecipitated with FH-CRBN (Fig. 2B). If CRBN functions as a substrate receptor of a Cul4-DDB1 E3 complex, it would be expected to compete for binding to DDB1 with other substrate receptor subunits, such as DDB2. Consistent with this, the amount of DDB1 coprecipitated with FH-CRBN was reduced in the presence of increasing amounts of coexpressed DDB2 (Fig. 2C). Although thalidomide can induce oxidative DNA damage (*4*), CRBN is likely to function independently of the DDB2-mediated DNA damage response pathway [see supporting online material (SOM) text].

We then examined whether the CRBN complex actually has E3 ubiquitin ligase activity. Because substrate receptors and Cul4 are known to undergo autoubiquitination in vitro in the absence of their specific substrates (*15*, *16*), in vitro ubiquitination assays were performed using purified protein components. Indeed, intrinsic ubiquitination activity was observed in the presence of the CRBN complex (fig. S4). We then examined whether CRBN is autoubiquitinated in cells. For this, CRBN was affinity-purified from 293T cells expressing FH-CRBN in the presence or absence of the proteasome inhibitor MG132. Autoubiquitination of FH-CRBN was detected in the presence of MG132, and its ubiquitination was abrogated by small interfering RNA (siRNA)–mediated depletion (knockdown) of Cul4A (Fig. 2D, fig. S5A, and table S2). Knockdown of DDB1 led to a substantial reduction of the CRBN protein level (fig. S5B), and it was not possible to determine the effect of DDB1 knockdown on CRBN ubiquitination. Nevertheless, this finding suggests that DDB1 and CRBN are functionally linked.

To further investigate the role of DDB1 in CRBN function, we obtained a CRBN mutant deficient in DDB1 binding. Mutational analysis revealed that deletion of amino acids 187 to 260 of CRBN (ΔMid) abolishes its interaction with DDB1 (fig. S6). ΔMid was therefore stably expressed in 293T cells and examined for its ubiquitination after MG132 treatment. Ubiquitination of ΔMid was reduced compared with wild-type CRBN (Fig. 2E). Collectively, these findings suggest that CRBN is a subunit of a functional E3 ubiquitin ligase complex and undergoes autoubiquitination in a Cul4A- and DDB1-dependent manner.

Inhibition of CRBN function by thalidomide. To investigate the structural basis of the CRBN-thalidomide interaction and its functional significance, we wished to obtain a CRBN point mutant that does not bind to thalidomide but is assembled into a functional E3 complex. Using a series of deletion mutants, we mapped its thalidomide-binding region to the C-terminal 104 amino acids, which corresponds to the most highly conserved region of the protein (figs. S7 and S8). Assuming that evolutionarily conserved residues may be important for thalidomide binding, we constructed a series of point mutants, and two point

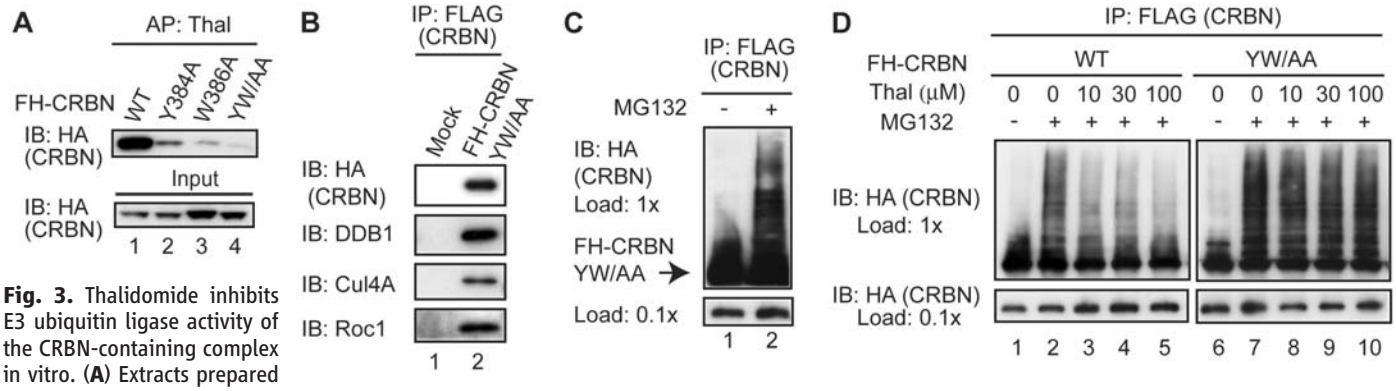

Fig. 3. Thalidomide inhibits E3 ubiquitin ligase activity of the CRBN-containing complex in vitro. (**A**) Extracts prepared from 293T cells overexpressing FH-CRBN or one of its mutants were incubated with thalidomide-immobilized beads, and lysates (input) and affinity-purified (AP) materials were immunoblotted (IB). (**B**) 293T cells stably expressing FH-CRBN$^{YW/AA}$ were subjected to FLAG-specific antibody immunoprecipitation (IP) and immunoblotting. (**C** and **D**) 293T cells stably expressing FH-CRBN or FH-CRBN$^{YW/AA}$ were processed as in Fig. 2E. In (D), cells were treated with the indicated concentrations of thalidomide for 4 hours before harvest.

mutants, Y384A and W386A, were found to be defective for thalidomide binding (Fig. 3A) (*11*). Moreover, the double point mutant Y384A/W386A (CRBN$^{YW/AA}$) had extremely low thalidomide-binding activity. We then asked whether CRBN$^{YW/AA}$ is functionally active in cells. The subcellular localization of the mutant was indistinguishable from wild-type CRBN (fig. S7C). Moreover, CRBN$^{YW/AA}$ was coprecipitated with DDB1, Cul4A, and Roc1 (Fig. 3B) and was autoubiquitinated after MG132 treatment (Fig. 3C), which demonstrated that CRBN$^{YW/AA}$ is assembled into a complete E3 ubiquitin ligase complex.

We examined possible effects of thalidomide on ubiquitination by treating 293T cells stably expressing FH-CRBN or FH-CRBN$^{YW/AA}$ with MG132 and thalidomide at similar or higher concentrations relative to the therapeutic doses used in humans (*21*). Autoubiquitination of wild-type CRBN was inhibited by thalidomide in a concentration-dependent manner, whereas autoubiquitination of CRBN$^{YW/AA}$ was not affected by thalidomide even at the highest concentration used (Fig. 3D). Together, these results suggest that thalidomide inhibits E3 function of the CRBN-containing complex by directly binding to CRBN.

CRBN as an in vivo target of thalidomide. Next, we investigated a possible role of CRBN in thalidomide teratogenicity in animal models. Thalidomide is teratogenic in rabbits and chicks, but not in mice and rats (*1*–*3*). We first used zebrafish as a model system because (i) the rapid progress of development of zebrafish can be monitored in real time because of the transparency of the embryo, (ii) knockdown of genes of interest can be carried out easily (*22*), and (iii) zebrafish are suitable for pharmacotoxicological studies (*23*). Given that thalidomide was recently shown to inhibit angiogenesis in zebrafish embryos (*24*), we reasoned that zebrafish might be susceptible to other activities of thalidomide.

To examine the effects of thalidomide on zebrafish development, we transferred dechorionated embryos to media containing different concentrations of thalidomide at 2 hours post fertilization (hpf) and allowed them to develop for 3 days. It was immediately apparent that in thalidomide-treated embryos, development of pectoral fins and otic vesicles was disturbed, whereas other aspects of development were not generally affected (Fig. 4, A and B, and fig. S9). More specifically, formation of the proximal endoskeletal disc of the pectoral fin was severely inhibited at 75 hpf (Fig. 4A), and otic vesicle size was significantly reduced at 30 hpf (Fig. 4B and fig. S11). Pectoral fin malformations were already apparent at 48 hpf (Fig. 5, C and D). More detailed phenotypes induced by thalidomide are described in the SOM text. Recent studies have suggested that development of pectoral fins and otic vesicles in teleosts share common molecular pathways with that of tetrapod limbs and ears (*25*–*27*).

Zebrafish have a *CRBN* orthologous gene which we call *zcrbn*, whose product has ~70% identity to human CRBN (fig. S8). We first examined the expression pattern of *zcrbn* mRNA and found that the gene is highly expressed in the brain, head vasculature, otic vesicles, and developing pectoral fins at 30 and 48 hpf (fig. S12). zCrbn interacts with DDB1 and is affinity-purified from zebrafish embryos as a major interactor with thalidomide (fig.

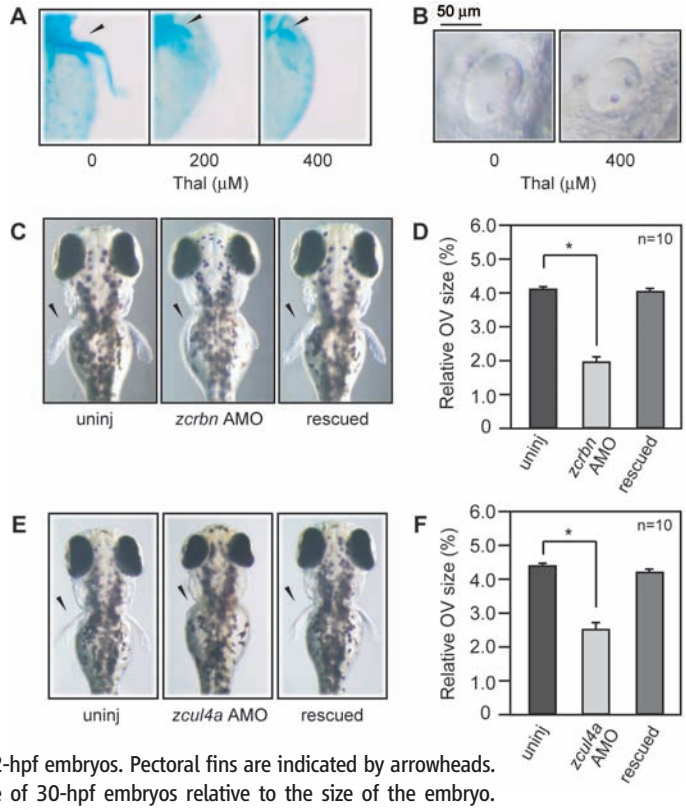

Fig. 4. Thalidomide treatment or down-regulation of the CRBN complex causes similar developmental defects in zebrafish. (**A** and **B**) Zebrafish embryos were allowed to develop in media containing the indicated concentrations of thalidomide. (A) Embryos at 75 hpf were fixed and stained with Alcian blue. Pectoral fins are indicated by arrowheads. (B) Close-up view of otic vesicles of 30-hpf live embryos. (**C** and **D**) Where indicated, *zcrbn* AMO was injected with (rescued) or without *zcrbn* mRNA into one-cell stage embryos. (**E** and **F**) Where indicated, *zcul4a* AMO was injected with or without *zcul4a* mRNA into one-cell stage embryos. (C and E) Dorsal views of pectoral fins of 72-hpf embryos. Pectoral fins are indicated by arrowheads. (D and F) Otic vesicle size of 30-hpf embryos relative to the size of the embryo. Representative raw data are shown in fig. S14. *$P < 0.001$. uninj, uninjected.

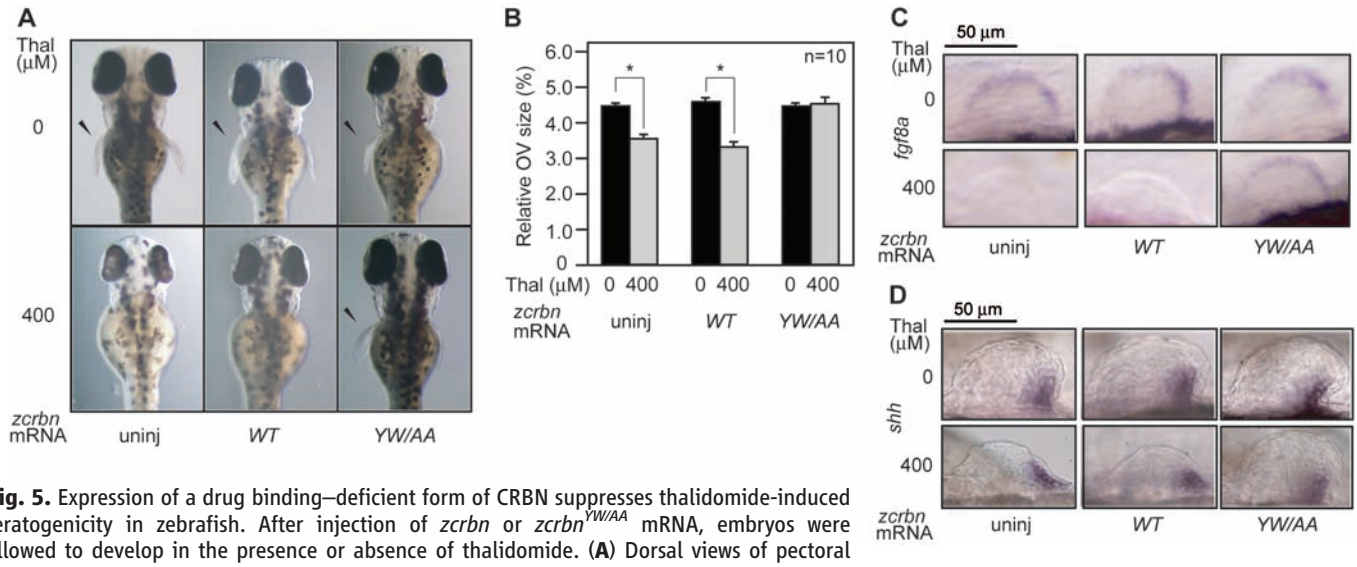

Fig. 5. Expression of a drug binding–deficient form of CRBN suppresses thalidomide-induced teratogenicity in zebrafish. After injection of *zcrbn* or *zcrbn*$^{YW/AA}$ mRNA, embryos were allowed to develop in the presence or absence of thalidomide. (**A**) Dorsal views of pectoral fins of 72-hpf embryos. Fins are indicated by arrowheads. (**B**) Otic vesicle size of 30-hpf embryos relative to the size of the embryo. *$P < 0.001$. (**C** and **D**) Embryos at 48 hpf were subjected to hybridization with antisense probes for *fgf8a* or *shh*. Close-up views of fin buds are shown. uninj, uninjected.

S13), which suggests that the findings of our cell culture studies are valid in zebrafish. Hence, the function of zCrbn during early development was examined. Embryos injected with an antisense morpholino oligonucleotide (AMO) for *zcrbn* exhibited specific defects in fin and otic vesicle development (Fig. 4, C and D, and figs. S9 to S11 and S14), phenotypes similar to those of thalidomide-treated embryos. For example, the size of otic vesicles was reduced by half in the knockdown embryos (Fig. 4D). These defects were rescued by coinjection of *zcrbn* mRNA (Fig. 4, C and D, and figs. S9 to S11 and S14).

The above findings suggested an interesting possibility that thalidomide exerts teratogenic effects by inhibiting zCrbn function. If so, its teratogenic effects might be reversed by overexpression of a functionally active, thalidomide binding–defective form of zCrbn. To test this idea, we used zCrbn carrying Y374A and W376A mutations, which correspond to Y384A and W386A mutations in human CRBN. zCrbn$^{YW/AA}$ had extremely low thalidomide-binding activity (fig. S13C). In the absence of thalidomide, overexpression of zCrbn or zCrbn$^{YW/AA}$ had no discernible effect on fin and otic vesicle development (Fig. 5 and figs. S9 to S11). As we have already seen in Fig. 4, thalidomide treatment significantly reduced otic vesicle size ($P < 0.001$, Mann-Whitney U test) (Fig. 5B and fig. S11). Thalidomide treatment of embryos overexpressing wild-type zCrbn similarly reduced otic vesicle size ($P < 0.001$). However, thalidomide treatment of embryos overexpressing zCrbn$^{YW/AA}$ did not affect otic vesicle size significantly ($P = 0.59$). Thalidomide-induced pectoral fin malformations were also rescued by overexpression of zCrbn$^{YW/AA}$ (Fig. 5A and fig. S10), which demonstrated that thalidomide exerts teratogenic effects by binding to CRBN and inhibiting its function.

Molecular mechanism of thalidomide teratogenicity. As the connection between thalidomide and CRBN was established, we then examined whether the CRBN-containing E3 complex is involved in thalidomide teratogenicity, by down-regulating the zebrafish homolog of Cul4A (zCul4a). *zcul4a* mRNA is abundantly expressed in the brain and pectoral fins (fig. S12). As expected, microinjection of AMO for *zcul4a* caused similar defects in otic vesicles and pectoral fins, and these phenotypes were rescued by coinjection of *zcul4a* mRNA (Fig. 4, E and F, and figs. S9 to S11 and S14). Nevertheless, phenotypic similarities between zCrbn and zCul4A knockdown embryos may be just coincidental. To rule out this possibility, we examined the importance of the physical interaction between CRBN and DDB1 in vivo, by using zCrbn$^{\Delta Mid\ YW/AA}$. As expected, DDB1 and thalidomide did not bind to this mutant, and thalidomide-induced developmental defects were not rescued by its overexpression (fig. S15). These results suggest that the CRBN-containing E3 ubiquitin ligase complex plays a crucial role in fin and otic vesicle development and is a target of thalidomide.

To obtain a clue to the pathway(s) downstream of thalidomide and CRBN, we examined expression of key signaling molecules during pectoral fin development. Sonic hedgehog (Shh) is expressed in the zone of polarizing activity (ZPA) and is responsible for anteroposterior patterning of limbs (*28*), whereas fibroblast growth factor (fgf) 8 is expressed in the apical ectodermal ridge (AER) of limbs and is responsible for limb outgrowth along the proximodistal axis (*29*, *30*). In thalidomide-treated 48-hpf embryos, *fgf8a* expression in the AER was severely reduced or absent (Fig. 5C), whereas *shh* expression in the ZPA was affected negligibly (Fig. 5D). In addition, *fgf8a* expression was restored by injection of *zcrbn*$^{YW/AA}$ mRNA (Fig. 5C). Knockdown of zCrbn or zCul4a also resulted in a reduction of *fgf8a* expression in the AER, whereas it had little effect on *shh* expression in the ZPA (fig. S14). Thus, an inhibitor of fgf8 production is a possible downstream target of thalidomide and the CRBN-containing E3 complex.

Conserved role for CRBN in zebrafish and chicks. Finally, in order to validate our findings, we used chicks, well-established model organisms for studying thalidomide teratogenicity. As reported previously (*12*, *31*), exposure to thalidomide resulted in the complete absence of a forelimb at a high incidence (Fig. 6A and fig. S16). Overexpression of human CRBN$^{YW/AA}$, but not wild-type CRBN, in the forelimb field remarkably reduced thalidomide sensitivity (Fig. 6A and fig. S16). Expression of *fgf8* and *fgf10* was then examined. Fgf10 is also an important regulator of proximodistal limb patterning and is normally expressed in the mesoderm beneath the AER (Fig. 6B). Thalidomide down-regulated *fgf10* expression in the mesoderm and, perhaps to a lesser extent, *fgf8* expression in the AER, and their expression was restored by overexpression of CRBN$^{YW/AA}$ (Fig. 6B). These results, together with the finding that chick CRBN binds to thalidomide and DDB1 (fig. S17), suggest that the developmental role of CRBN is conserved in fins and limbs.

Discussion. The mechanism of action of thalidomide appears to be multifaceted, but is not fully understood. The immunomodulatory and antiangiogenic activities of thalidomide have been proposed to be partly responsible for its teratogenic activity, as well as its therapeutic value in the treatment of leprosy and multiple myeloma (*2*, *3*, *6*, *7*). In this respect, thalidomide is known to inhibit the production of some cytokines such as tumor necrosis factor–α and vascular endothelial growth factor (*32*, *33*). Thalidomide is also capable of inducing apoptosis and producing reactive oxygen species (*3*, *4*). Despite such accumulating data, little is known about direct

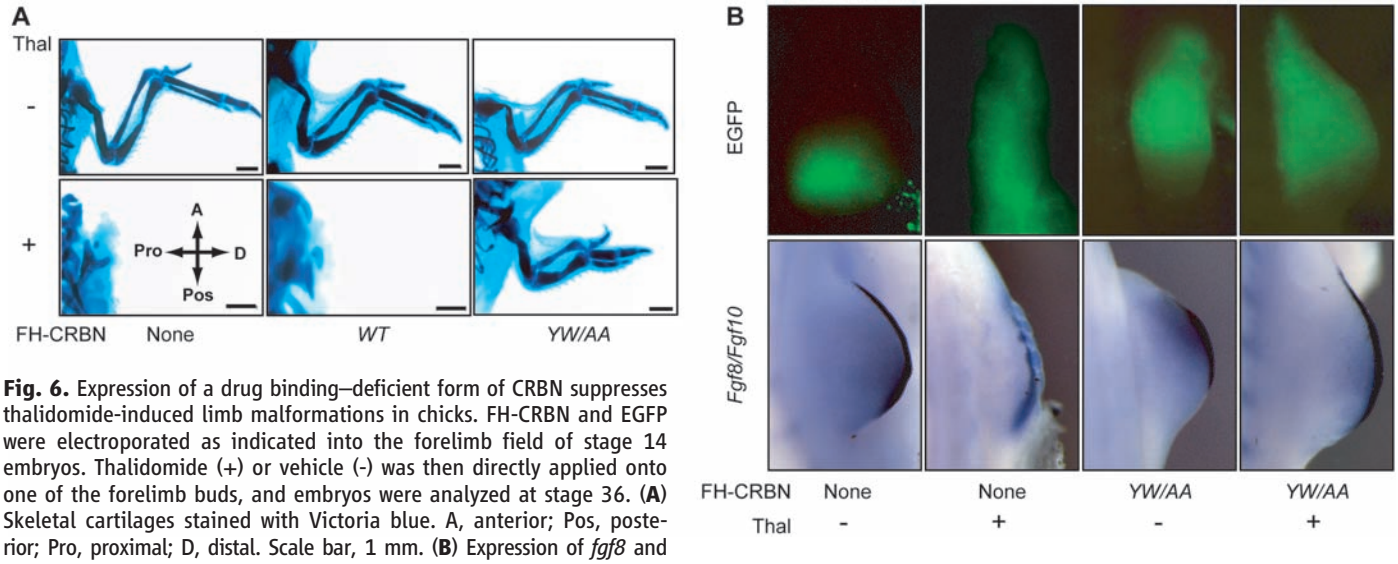

Fig. 6. Expression of a drug binding–deficient form of CRBN suppresses thalidomide-induced limb malformations in chicks. FH-CRBN and EGFP were electroporated as indicated into the forelimb field of stage 14 embryos. Thalidomide (+) or vehicle (-) was then directly applied onto one of the forelimb buds, and embryos were analyzed at stage 36. (**A**) Skeletal cartilages stained with Victoria blue. A, anterior; Pos, posterior; Pro, proximal; D, distal. Scale bar, 1 mm. (**B**) Expression of *fgf8* and *fgf10* visualized by in situ hybridization. EGFP marks area of electroporation.

molecular targets of thalidomide. Here we provided several lines of evidence that CRBN is a primary target of thalidomide teratogenicity. Because overexpression of the thalidomide-insensitive form of CRBN rescued the effects of thalidomide largely, if not entirely, in zebrafish and chicks, CRBN is thought to play an important role as an upstream mediator of thalidomide action at least in these species. Whereas CRBN is ubiquitously expressed in humans, thalidomide exerts tissue-specific effects. Evidently, CRBN is necessary, but not sufficient, for thalidomide teratogenicity, and downstream components are likely to contribute to the tissue-specific effects of thalidomide (see SOM text).

The finding that fgf8 is a downstream target of thalidomide and CRBN fits well with a previous report, in which a similar effect of thalidomide on *fgf8* expression was described in rabbits, another sensitive species (*34*). In developing chick limb buds, thalidomide was shown to up-regulate expression of a subset of bone morphogenetic protein (BMP) family genes and to induce apoptosis (*12*). Coincidentally, mouse BMPs were shown to inhibit *fgf8* expression and to induce apoptosis in the AER (*35*). Thus, CRBN appears to be a missing link between thalidomide and these key developmental regulators.

However, this study does not rule out other mechanisms of thalidomide action, particularly in mammals. Thalidomide-induced oxidative stress is thought to occur through the direct formation of reactive oxygen species (*4*) and is therefore clearly a CRBN-independent process. Second, a recent study suggested antiangiogenic activity of thalidomide as a primary cause of chick limb malformations, demonstrating that thalidomide-induced inhibition of vasculogenesis precedes inhibition of *fgf8* expression and cell death in limb buds (*31*). By contrast, our data suggest that, in zebrafish, inhibition of vasculogenesis follows thalidomide-induced morphological and transcriptional changes in pectoral fin buds (fig. S18 and SOM text), which implies that the sequence of events induced by thalidomide is different in these organisms. These observations are concordant with the common view of species differences in thalidomide action (see SOM for further discussion on the species differences). Another point to consider is the fact that thalidomide is rapidly hydrolyzed or metabolized to more than a dozen products in vitro and in vivo (*2*, *21*, *36*). Thalidomide and its products may have the same or different molecular target(s) (see SOM text).

Our findings suggest that thalidomide exerts teratogenic effects, at least in part, by binding to CRBN and inhibiting the associated ubiquitin ligase activity (fig. S19). We speculate that control of ubiquitin-dependent proteolysis by thalidomide and CRBN leads to abnormal regulation of the BMP and fgf8 signaling pathways and of developmental programs that require their normal functions. Incidentally, many E3 ubiquitin ligases are known to target developmental and/or transcriptional regulators and to control developmental programs (*37*, *38*). There are, however, a number of unanswered questions, such as: What are the substrates of CRBN E3 ubiquitin ligase? How does thalidomide inhibit the ubiquitination of CRBN in the ligase complex? How might this pathway be interconnected to the other pathways targeted by thalidomide? These issues need to be addressed to fully appreciate the model. Last, but not least, because thalidomide is now used for the treatment of multiple myeloma and leprosy, identification of its direct target may allow rational design of more effective thalidomide derivatives without teratogenic activity (see SOM text).

References and Notes

1. M. T. Miller, K. Strömland, *Teratology* **60**, 306 (1999).
2. M. Melchert, A. List, *Int. J. Biochem. Cell Biol.* **39**, 1489 (2007).
3. J. Knobloch, U. Rüther, *Cell Cycle* **7**, 1121 (2008).
4. T. Parman, M. J. Wiley, P. G. Wells, *Nat. Med.* **5**, 582 (1999).
5. R. J. D'Amato, M. S. Loughnan, E. Flynn, J. Folkman, *Proc. Natl. Acad. Sci. U.S.A.* **91**, 4082 (1994).
6. J. Sheskin, *Clin. Pharmacol. Ther.* **6**, 303 (1965).
7. S. Singhal *et al.*, *N. Engl. J. Med.* **341**, 1565 (1999).
8. J. B. Zeldis, B. A. Williams, S. D. Thomas, M. E. Elsayed, *Clin. Ther.* **21**, 319 (1999).
9. S. Sakamoto, Y. Kabe, M. Hatakeyama, Y. Yamaguchi, H. Handa, *Chem. Rec.* **9**, 66 (2009).
10. Materials and methods and additional text are available as supporting information on *Science* Online.
11. Single-letter abbreviations for the amino acid residues used in this research article are as follows: A, Ala; C, Cys; D, Asp; E, Glu; F, Phe; G, Gly; H, His; I, Ile; K, Lys; L, Leu; M, Met; N, Asn; P, Pro; Q, Gln; R, Arg; S, Ser; T, Thr; V, Val; W, Trp; and Y, Tyr.
12. J. Knobloch, J. D. Shaughnessy Jr., U. Rüther, *FASEB J.* **21**, 1410 (2007).
13. J. J. Higgins, J. Pucilowska, R. Q. Lombardi, J. P. Rooney, *Neurology* **63**, 1927 (2004).
14. S. Angers *et al.*, *Nature* **443**, 590 (2006).
15. R. Groisman *et al.*, *Cell* **113**, 357 (2003).
16. F. Ohtake *et al.*, *Nature* **446**, 562 (2007).
17. C. M. Pickart, *Cell* **116**, 181 (2004).
18. M. D. Petroski, R. J. Deshaies, *Nat. Rev. Mol. Cell Biol.* **6**, 9 (2005).
19. K. Sugasawa *et al.*, *Cell* **121**, 387 (2005).
20. J. Jin, E. E. Arias, J. Chen, J. W. Harper, J. C. Walter, *Mol. Cell* **23**, 709 (2006).
21. M. E. Franks, G. R. Macpherson, W. D. Figg, *Lancet* **363**, 1802 (2004).
22. A. Nasevicius, S. C. Ekker, *Nat. Genet.* **26**, 216 (2000).
23. M. B. Veldman, S. Lin, *Pediatr. Res.* **64**, 470 (2008).
24. T. Yabu *et al.*, *Blood* **106**, 125 (2005).
25. M. Tanaka *et al.*, *Nature* **416**, 527 (2002).
26. M. C. Davis, R. D. Dahn, N. H. Shubin, *Nature* **447**, 473 (2007).
27. A. Streit, *J. Anat.* **199**, 99 (2001).
28. R. D. Riddle, R. L. Johnson, E. Laufer, C. Tabin, *Cell* **75**, 1401 (1993).
29. A. M. Moon, M. R. Capecchi, *Nat. Genet.* **26**, 455 (2000).
30. M. Lewandoski, X. Sun, G. R. Martin, *Nat. Genet.* **26**, 460 (2000).
31. C. Therapontos, L. Erskine, E. R. Gardner, W. D. Figg, N. Vargesson, *Proc. Natl. Acad. Sci. U.S.A.* **106**, 8573 (2009).
32. A. L. Moreira *et al.*, *J. Exp. Med.* **177**, 1675 (1993).
33. D. Gupta *et al.*, *Leukemia* **15**, 1950 (2001).
34. J. M. Hansen, S. G. Gong, M. Philbert, C. Harris, *Dev. Dyn.* **225**, 186 (2002).
35. S. Pajni-Underwood, C. P. Wilson, C. Elder, Y. Mishina, M. Lewandoski, *Development* **134**, 2359 (2007).
36. F. Chung *et al.*, *Clin. Cancer Res.* **10**, 5949 (2004).

37. Y. Cang *et al.*, *Cell* **127**, 929 (2006).
38. Y. Cang *et al.*, *Proc. Natl. Acad. Sci. U.S.A.* **104**, 2733 (2007).
39. We thank T. Wada, S. Sakamoto, and S. Ishihara for discussions; P. Raychaudhuri, T. Matsunaga, S. Krauss, B. Thisse, A. Kawakami, S. Noji, J. Izpisua-Belmonte, K. Kawakami, and J. Yamauchi for valuable reagents; Y. Tsuboi for technical support; and P. Sharp and A. Berk for comments on this manuscript. This work was supported by Special Coordination Funds for Promoting Science and Technology from JST, by the Global COE (Center of Excellence) Program from the Japan Ministry of Education, Culture, Sports, Science, and Technology (MEXT), and by a grant for Research and Development Projects in Cooperation with Academic Institutions from the New Energy and Technology Development Organization (H.H. and H.A.). This work was also supported by grants-in-aid for Scientific Research (20370084 to T.O.) and for Young Scientists (21770226 to T.S.) from MEXT and by the Precursory Research for Embryonic Science and Technology program from JST (T.S.). T.I. was a Japan Society for the Promotion of Science Research Fellow. An application for a patent has been filed in the Japan Patent Office.

Supporting Online Material
www.sciencemag.org/cgi/content/full/327/5971/1345/DC1
Materials and Methods
SOM Text
Figs. S1 to S19
Tables S1 and S2
References

5 June 2009; accepted 10 February 2010
10.1126/science.1177319

REPORTS

Variations in the Sun's Meridional Flow over a Solar Cycle

David H. Hathaway[1]* and Lisa Rightmire[2]

The Sun's meridional flow is an axisymmetric flow that is generally directed from its equator toward its poles at the surface. The structure and strength of the meridional flow determine both the strength of the Sun's polar magnetic field and the intensity of sunspot cycles. We determine the meridional flow speed of magnetic features on the Sun using data from the Solar and Heliospheric Observatory. The average flow is poleward at all latitudes up to 75°, which suggests that it extends to the poles. It was faster at sunspot cycle minimum than at maximum and substantially faster on the approach to the current minimum than it was at the last solar minimum. This result may help to explain why this solar activity minimum is so peculiar.

The Sun's meridional flow has been difficult to measure (*1*). Its amplitude (10 to 20 m s^{-1}) is more than an order of magnitude weaker than that of the other major flows on the surface of the Sun (granulation ~3000 m s^{-1}, supergranulation ~300 m s^{-1}, and differential rotation ~170 m s^{-1}). In the past, this has led to reports of vastly different flow speeds and directions (*2*–*5*). Despite its weakness, the meridional flow plays a key role in the magnetic evolution of the Sun's surface. It transports magnetic elements that, when carried to the poles, reverse the magnetic polarity of the poles and build up polar fields of opposite polarity after each sunspot cycle maximum. Models of this magnetic flux transport process (*6*–*8*) have employed a variety of substantially different flow profiles. The fidelity of these flux transport models is important because they are used in climate change studies (*9*, *10*) to estimate the total irradiance of the Sun over the past century. The meridional flow is also key to flux transport dynamo models that have been used to predict the amplitude of Solar Cycle 24 (*11*, *12*). An obvious conflict between the surface flux transport models (*6*–*10*) and the flux transport dynamo models (*11*, *12*) is found in their sensitivity to the strength of the meridional flow. A stronger meridional flow produces weaker polar fields in the surface flux transport models, whereas the same flow produces stronger polar fields (and shorter sunspot cycles) in the flux transport dynamos. Solar Cycle 23 (1996 to 2008) provides an interesting problem for all of these models. The strength of the polar fields produced after cycle maximum in 2000–2001 was only about half that seen in the previous three solar cycles (*13*). Furthermore, cycle 24 started much later than average. The late start for cycle 24 has left behind a long quiet minimum unlike any in the past 100 years.

We measured the Sun's meridional flow to determine its variability over Solar Cycle 23 by following the motions of the small magnetic elements that populate the entire surface of the Sun. These are precisely the elements whose motions are modeled in both the surface flux transport models and the flux transport dynamo models. Motions of sunspots, and even the plasma at the surface, are known to differ from those of the small magnetic elements (*1*–*5*). The data we used have been acquired by the Michelson Doppler Imager (MDI) on the European Space Agency (ESA)/National Aeronautics and Space Administration (NASA) Solar and Heliospheric Observatory (SOHO). MDI produces images of the line-of-sight magnetic field across the visible solar disc every 96 min. This is done by measuring differences in circular polarization on either side of a spectral absorption line caused by traces of nickel in the Sun's atmosphere (*14*). We measured the displacement of the magnetic elements by comparing their positions at 8-hour (5-image) intervals from May 1996 to June 2009. The 1024-by-1024 pixel magnetic images were mapped onto a 1024-by-1024 grid in heliographic latitude and longitude from the central meridian. This mapping accounts for changes in the position angle of the Sun's rotation axis relative to the spacecraft's vertical axis, changes in the tilt angle of the Sun's rotation axis toward or away from the spacecraft, and changes in perspective at different distances from the Sun. Because sunspots have very different proper motions (*4*) and produce localized outflows (*15*), we removed sunspots and their immediate surroundings by masking all pixels with measured absolute field strengths greater than 500 Gauss and all contiguous pixels of the same polarity with absolute field strengths above 100 Gauss. Displacements in longitude and

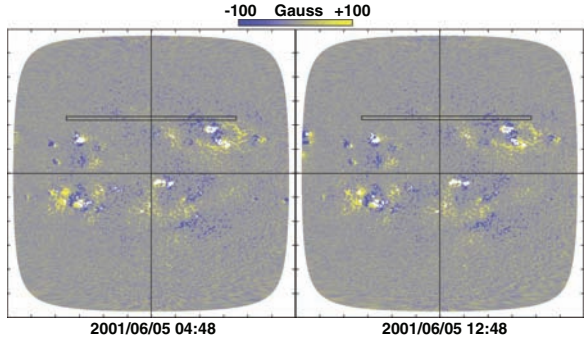

Fig. 1. Magnetic element motion. A pair of masked magnetic maps from 5 June 2001 that were obtained 8 hours apart are shown here with blue representing negative magnetic polarity and yellow representing positive magnetic polarity. The tick marks around the borders are at 15° intervals in latitude and in longitude from the central meridian. The masked-out sunspot areas are evident as white patches. The strongest correlation for the outlined strip of pixels in the earlier map (**left**) is calculated to occur for a shift of 23.7 pixels in longitude and 0.4 pixels in latitude for a similar strip in the later map (**right**).

[1]NASA Marshall Space Flight Center, Huntsville, AL 35812, USA. [2]University of Memphis, Memphis, TN 38152, USA.

*To whom correspondence should be addressed. E-mail: david.hathaway@nasa.gov